NATIONAL ACADEMY OF SCIENCES

Number 53 • November 1961

IGY BULLETIN

A monthly survey of plans, activities and findings in geophysics—with emphasis on United States contributions to the International Geophysical Year, International Geophysical Cooperation–1959, and similar international endeavors including the World Magnetic Survey, the Year of the Quiet Sun, the Indian Ocean Expedition, the Antarctic research program, and space exploration and research. Preparation and publication of the Bulletin *is supported by the National Science Foundation.*

US Antarctic Meteorology during the IGY

Part I: Little America and Amundsen-Scott Stations

The following material is based on a series of reports by US Weather Bureau meteorologists who participated in the IGY meteorological program in the Antarctic. The original reports appeared in various issues of Weatherwise, *a publication of the American Meteorological Society, and are referenced separately in the Bibliographic Notes of this* Bulletin. *The most recent report of the series, on IGY meteorology at the USSR Mirny Station, served as the basis for a report in* Bulletin No. 52; *earlier reports on IGY Antarctic meteorological studies appeared in* Bulletin Nos. 15 *and* 24.

The widespread network of year-round scientific stations established in the Antarctic as part of the IGY program made it possible, for the first time in history, for meteorologists to obtain a broad range of synoptic weather data in that vast, frigid, hitherto little-known portion of the earth's surface. In addition to providing knowledge of the unique weather and climate of Antarctica itself, these studies have provided new insights into atmospheric processes and circulation in general and have improved weather forecasting throughout the Southern Hemisphere. Part I of this report reviews the accomplishments and findings of meteorologists at Little America and Amundsen-Scott Stations during the IGY period (1957–1958), and Part II, which will appear in *Bulletin No. 54,* reviews the work at Hallett Station, manned jointly by US and New Zealand personnel, Byrd Station, and the Antarctic Weather Central.

Little America IGY Station

The USNC-IGY meteorological observation program at Little America IGY Sta-

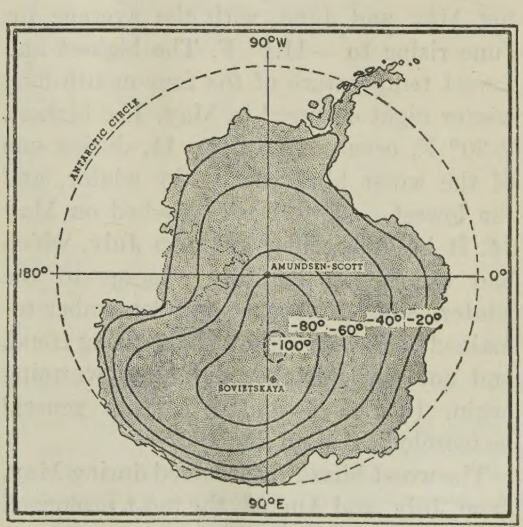

Fig. 1. *Isotherms Showing Distribution of Average Surface Temperatures (in °F) for an Antarctic Winter Month—June 1958.*

Table 1. *Little America Temperature and Precipitation Data, 1957.*

Month	Temperature (°F)					Precipitation (inches of water equivalent)		Snow, Sleet (in inches)		
	Monthly averages	Highest	Dates	Lowest	Dates	Total	Greatest in 24 hrs.	Total	Greatest in 24 hrs.	Dates
Feb	10.3	30	6	−17	19	0.67	0.53	9.5	6.0	23
Mar	−14.7	15	4,20,21	−49	31	0.66	0.25	5.6	1.7	27
Apr	−27.0	10	10	−55	27	0.36	0.13	3.6	1.3	9
May	−23.4	30	11	−63	24	2.31	0.86	22.1	7.6	8–9
June	−11.1	25	15	−51	10	1.50	0.40	15.6	4.0	16
July	−32.0	6	24	−61	10	0.37	0.12	3.7	1.2	20–21
Aug	−30.1	0	29	−56	2,26	0.19	0.06	2.2	0.6	29
Sept	−29.3	−3	14	−51	13	0.32	0.07	2.8	0.7	4–5
Oct	−3.2	29	27	−43	1	1.28	0.31	13.6	3.7	5–6
Nov	9.4	30	30	−16	14	0.58	0.27	5.5	2.8	1–2

tion, Antarctica, began on January 30, 1957, a few hours after the observing personnel had been flown in by helicopter from the *USS Curtiss,* in Kainan Bay.

February at Little America was comparatively mild, making it not too unpleasant to work outside during most of the month. Temperatures fell rapidly during March and April, and the average for April was —27° F. A warming trend followed, during May and June, with the average for June rising to —11.1° F. The highest and lowest temperature of the four-month-long winter night occurred in May. The highest, +30° F, occurred on May 11, during one of the worst blizzards of the winter, and the lowest, —63° F, was reached on May 24. It became colder again in July, which had the lowest monthly average of the winter, —32° F. August and September remained cold, with only a slight rising trend, and not until October did rapid warming begin. (Tables 1 and 2 contain general meteorological data for 1957.)

The worst blizzards occurred during May, June, July, and August, the most prolonged one beginning on May 8 and, except for a few short lulls, continuing until the 15th. On May 8, the temperature read —48° F and the wind blew from the southeast, continuing from that quadrant almost steadily until the 11th, when it shifted to the north-northeast and increased in speed. The air then became much warmer and more humid, with the temperature rising to +30° F for a short time. This blizzard caused heavy drifting of snow in the camp area, covering the buildings entirely except for the smokestacks protruding through the snow. The strongest blizzard winds struck near the end of August 1957, with 75-mph winds recorded on the 30th.

Before winter was over, the camp was covered by six feet of snow in places and only a few buildings were not completely buried. However, although snowdrifts accumulated quite rapidly in the vicinity of the station during blizzards, the accumulation in level unobstructed areas a mile or more away was probably not greater than 10–15 inches during the year. The greatest snowfalls not associated with blizzards occurred during February and again in October. This snow, of lower density and softer than the hard, packed snow that accumulated during blizzards, was much more difficult to walk on.

Monthly snow accumulation for most of

Table 2. *Little America Wind and Cloud-Cover Data, 1957.*

Month	Wind					Cloud Cover (Number of days)		
	Average hourly speed*	Prevailing direction	Maximum speed**	Direction of max. wind	Date of max. wind	Clear	Partly cloudy	Cloudy
Feb	9.3	SE	—	—	—	1	11	16
Mar	13.5	SE	35	SE	21	4	8	19
Apr	11.7	S	42	N	10	10	7	13
May	15.9	SE	61	NE	14	15	0	16
June	17.3	SE	54	NE	13,14	5	8	17
July	14.5	SE	39	NE	24	10	10	11
Aug	16.2	SE	75	N	30	9	14	8
Sept	12.0	SE	25	NE	14	7	13	10
Oct	17.6	SE	52	NE	7	2	9	20
Nov	11.1	SE	39	N	1	8	5	17
	*knots		**mph					

1957 is shown in Table 1. The accumulation values of 22.1 inches for May and 15.6 inches for June are probably not representative as the measurements were made too near the camp. The snow-stake readings for these months show much less accumulation (Table 3). Because of the rapid build-up of snow cover during February, it was thought that the annual cover would be quite deep. Instead of a continuing rapid pile-up, however, a strong southwesterly wind came up on March 2, and in several hours almost 6 inches of snow had been eroded from the snow cover and blown away, leaving the surface very hard and rough. Where the snow had been compacted by the passage of people or vehicles, it was left several inches above the surrounding surfaces. In general, accumulation during the blizzard months was rather light and it was not until October that the snow surface, as shown by snow-stake readings, again reached its March 1 level.

September was mostly fair and cold, but there was much cloudiness and snowfalls were frequent in October and the first few days of November, restricting aircraft flights and other outside activities. Conditions then improved and there were many sunny days during the remainder of November.

Density measurements of newly-fallen snow were begun in June 1957 and continued until the first part of November, after which no further accumulations occurred that were deep enough to measure. (See Table 4.) After a number of density meas-

Table 3. *Snow Stake Readings at Little America Station.*

Date (1957)	Stake No. 1	Stake No. 2	Stake No. 3	Stake No. 4	Average net accumulation between readings
Mar 1	0	0	0	0	0
Mar 3	− 6	−6	−4.5	−6	−5.6
Mar 30	− 3	−2	−1	−5	+2.9
Apr 2	− 4	−3	−2	−6	−1.0
May 2	− 3	−2	−1	−5	+1.0
May 31	− 4	+1	−2	−6	0.0
July 1	− 1	+1	−2	−6	+0.8
Aug 1	+ 2	+1	0	−4	+1.8
Aug 31	+ 1	+1	0	−5	−0.5
Sept 30	+ 1	+1	0	−5	0.0
Nov 1	+12	+7	+2	−2	+5.5
Nov 30	+14	+6	+3	0	+1.0
(Accumulation is measured in inches.)					Total +5.9

Note: The first snow stake was located approximately 500 feet north of the meteorology building and the other three, 200–250 yards apart, formed a straight line running north-northeast from the first. The first three stakes were on an almost level plane while the fourth was on the southern slope of a crevasse valley. The effect of nearness to the camp can be seen on the first two.

Table 4. *Density of Newly Fallen Snow or Snowdrift at Little America Station.*

Date (1957)	Length of core (inches)	Density	Wind range or average velocity (knots) during estimated period of accumulation
June 2	12.0	.208	
June 12	6.5	.077	
June 12	15.5	.178	
July 14	10.0	.269	18–29
July 24	12.0*	.329	25–35
July 30	13.5*	.237	15–25
Aug 1	24.0	.282	23–30
Aug 15	9.0	.145	12–21
Aug 31	24.0**	.437	45
Oct 8	24.0*	.344	32
Oct 23	7.4**	.181	19
Nov 1	24.0	.263	23
Nov 2	17.0	.320	

* Average of two samples
** Average of three samples
Note: Due to the small accumulations of snow on level surfaces, most samples were taken on the leeward side of objects, where sufficient depths accumulated to measure.

urements had been made, it was realized that there might be some correlation between snow density and the speed of the wind while the snow was accumulating. Thereafter, attempts were made to determine the range of wind speeds, or the average speed, during periods when snow was accumulating. This is rather difficult to do as drifts shift from time to time and it is difficult to determine just when a particular drift started to build up. From the few readings obtained, it appears that densities ranged from about 0.1 or less with very light winds (not over 10 knots) and increased by about 0.1 for each 10-knot increase in wind speed up to about 40 or 50 knots. However, not enough readings could be made to determine precisely the nature of this relationship between snow density and wind speed, or whether the temperature might also have some effect on the density.

Frost formation at Little America was very heavy at times, especially during the fall and early spring. Feathery hoar frost, an inch or more thick, occasionally formed on exposed equipment and had to be removed periodically to permit the instruments to function properly.

During periods of high outgoing radiation, the temperature at the snow surface was sometimes 20°–30° F colder than at a height of 50 feet. On one occasion, a difference of 34° F was noted within a small vertical interval.

In general, weather conditions at Little America Station during the IGY were found to be better than expected. Blizzards are the most unpleasant weather phenomena in the Antarctic and create the greatest problems. They often occur unexpectedly and continue for many days, making it almost impossible for men to function outdoors and covering up exposed instruments, buildings, and supplies.

Amundsen-Scott IGY Station

The Amundsen-Scott Station was established at the geographic South Pole, about 9200 feet high (but at a pressure altitude of about 10,500 feet) on the Polar Plateau about 800 miles from Little America Station.

By late April 1957, nearly all meteorological equipment had been installed and was operating at the South Pole Station. The twilight period was over and four months of complete darkness had begun, to be broken only by the appearance of the moon for several days each four weeks. Eight months of winter isolation had begun in mid-February with the departure of the last plane. Temperatures that had been in the —10° to —20° F range in mid-January dropped steadily to the —60° to —80° F range by mid-March and then leveled off. From April through October 1957, the temperature measured at a depth of 30 feet below the snow surface varied by less than 1° F from its mean value of —58.5° F. Table 5 gives weather data for the South Pole Station in 1957.

The meteorological program at Amundsen-Scott Station during this winter period included measurements of snowfall using a gauge mounted on the wind mast, 30 feet

Table 5. *Meteorological Data for Amundsen-Scott Station, 1957.*

Month	Temperature (°F)					Pressure (mb)					Wind					Cloud cover (Number of Days)		
	Average	Highest	Date	Lowest	Date	Average	Highest	Date	Lowest	Date	Average hourly speed (mph)	Prevailing direction	Maximum Speed (mph)	Direction of Max. wind	Date of Max. wind	Clear	Partly cloudy	Cloudy
Jan 9–31	−18.1	− 6.0	11	− 29.8	26	687.8	697.3	11	681.0	27	11.3	0°				3	14	6
Feb	−36.8	−18.0	5	− 69.2	28	681.0	696.4	16	671.2	28	11.4	0°				11	6	11
Mar	−64.7	−35.0	19	− 82.5	29	681.7	695.6	17	664.6	26	13.4	23°E	32	45°E	23, 24	8	12	11
Apr	−69.7	−25.6	6	− 89.1	19	681.7	692.9	30	669.8	14	17.3	23°E	39	23°E	5	17	10	3
May	−68.3	−30.1	15	−100.4	12	684.2	713.2	27	667.5	19	17.2	23°E	54	23°E	25	19	8	4
June	−69.6	−42.3	12	− 97.0	18	685.7	701.3	15	671.5	12	19.1	45°E	38	23°E	10, 25	27	3	0
July	−77.5	−40.7	3	− 98.8	29	673.2	683.0	16	657.3	30	17.4	23°E	43	23°E	3, 4, 5	23	6	2
Aug	−72.7	−45.4	4	− 99.7	27	682.0	703.0	6	657.3	1	18.0	23°E	38	23°E	1	20	8	3
Sept	−80.1	−57.7	30	−102.1	18	677.3	684.7	7	663.1	2	14.7	90°E	42	45°E	29	19	8	3
Oct	−62.9	−45.4	18	− 86.1	3	677.3	682.4	7	670.2	20	15.8	23°E	39	23°E	12	12	16	3
Nov	−34.4	− 2.2	22	− 54.6	1	688.5	700.3	23	677.3	7	10.9	23°E	32	23°E	23	18	10	2
Dec	−13.4	− 2.0	15	− 21.5	3	693.5	704.7	18	681.0	30	8.2	23°E	22	23°E	17	14	10	7
Year	−55.7					682.8					14.5							

above the snow surface. This was an attempt to obtain more accurate measurements of falling snow, since records of the amount collected on the surface are always biased by an unknown amount of drifting snow. Table 6 shows precipitation for the winter of 1957, in terms of both solid amounts of snow (S.A.) and of water equivalents (W.E.), for gauges on the ground and on the 30-foot mast. Replicas of falling snow crystals were also made when conditions permitted. The types of crystals most frequently observed were bullets (rod-like forms) and skeleton plates (flat, branching, star-shaped forms).

Interesting features of the Antarctic stratosphere are the gradual cooling from February into August and the very rapid warming in October-November. In 1957, the cooling trend culminated in minimum stratospheric temperatures of —90° to —93° C, measured at altitudes of about 18–20 km in late July and early August.

Early in the year, the wind was rarely calm and, surprisingly, as winter approached the average wind speed increased. In the 720 hourly observations made during June, for example, no wind speeds of less than 6 knots or of more than 30 knots were recorded. June was the windiest month in the sense that it had the highest average speed (19.1 mph) but it was a typical win-

Table 6. *Precipitation at the South Pole Station, Winter 1957.*

Location of gauge	July		August		September		October	
	S.A.*	W.E.**	S.A.	W.E.	S.A.	W.E.	S.A.	W.E.
Surface	6.9″	1.45″	10.5″	1.50″	1.6″	0.36″	23.5″	6.67″
30 feet above surface	0.5″	0.09″	1.4″	0.12″	0.3″	0.04″	0.35″	0.04″

* Solid amounts ** Water equivalents

Table 7. *Winds at Amundsen-Scott Station, June 1957.*

	Speed (knots)								Nr. hours	Frequency (% of time)	Average speed
	Calm	1–5	6–10	11–15	16–20	21–25	26–30	>30			
Calm	0	—	—	—	—	—	—	—	0	0	—
N (0°)		0	0	2	1	0	0	0	3	0.4	15.0
NNE (22°E)	—	0	3	26	63	63	6	0	149	20.7	19.4
NE (45°E)	—	0	3	63	121	56	2	0	245	34.0	17.9
ENE (77°E)	—	0	12	66	61	8	0	0	147	20.4	15.4
E (90°E)	—	0	13	115	20	0	0	0	148	20.6	13.5
ESE (112°E)	—	0	2	21	5	0	0	0	28	3.9	13.8
SE-NNW	—	0	0	0	0	0	0	0	0	0	—
Total hrs.	0	0	31	293	271	117	8	0	720	Monthly average speed	16.6
Frequency (% of time)	0	0	4.3	40.7	37.6	16.3	1.1	0			

ter month as far as the distributions of speed and direction were concerned. (See Table 7.)

Even periods of extreme cold were frequently accompanied by winds of moderate speed. The most severe day in this respect was July 29, when the average temperature was —94° F, with a high of —90° and a low of —99°, yet the average hourly wind speed for the day was 16.4 knots. Under such conditions, an exposed nose or cheek can be frozen in seconds if the mistake is made of facing into the wind.

The wind observations also showed that nearly all of the coldest days occurred when the wind blew from 90° E. This implied the existence of higher terrain and a colder climate in that direction, the advective effects of which were not entirely compensated by the adiabatic heating of the descending air. As indicated in Figure 1, a map of the isotherms of average surface temperature for June 1958, the "cold pole" of Antarctica probably is situated somewhere between the US South Pole Station and the USSR Sovietskaya Station.

Meterological Applications of Explorer VII Infrared Radiation Measurements

The following material is based on a more-detailed report, by Lt. Col. Melvin Weinstein, USAF Air Weather Service, and Verner E. Suomi, Department of Meteorology, University of Wisconsin, which appears in the US Weather Bureau's Monthly Weather Review, *November 1961.*

The radiation-balance experiment aboard IGY satellite Explorer VII (1959 Iota) was designed to measure solar, reflected, and terrestrial radiation currents in order to determine the radiant heat flow to and from the earth and, ultimately, to obtain a clearer understanding of the driving force behind the circulation of the atmosphere. A report in *Bulletin No. 52* describes the background, instrumentation, and techniques of the Explorer VII infrared radiation experiment and presents earlier results of analyses of the data obtained, which show large-scale radiation patterns around the earth and indicate an apparent relationship between these radiation patterns and large-scale surface weather patterns.

In the continuing work on which the pres-

ent report is based, these initial studies were carried further by comparing Explorer VII maps of long-wave radiation loss with composite nephanalyses (cloud-cover analyses) as well as with frontal analyses, and by plotting on a single map the locations and patterns of movement of radiation centers and lower-atmosphere pressure centers.

Results of these continuing studies definitely confirm a correspondence between radiation centers and near-surface low- and high-pressure centers with respect to location, 24-hour intensifications and movements, and the conformity of these movements to the geostrophic flow at the 500-milibar level (about 19,000 feet). (Geostrophic flow is horizontal frictionless flow of air in which the apparent force arising from the earth's rotation exactly balances the horizontal force resulting from pressure differences.) Potential weather-analysis and forecasting applications are also discussed.

Analysis Procedure

Because the spherical infrared sensor integrates the radiation over a large segment of the earth, composite radiation maps could be drawn using data from successive satellite passes, even though the passes were about 1 hour and 40 minutes apart. Isolangleys, lines of equal long-wave radiation loss expressed in langleys per minute $\times 10^{-3}$ are shown on the radiation maps (1 langley, ly, equals 1 gram-calorie/cm^2).

As the radiation maps are not synoptic, composite surface-frontal and nephanalysis maps coinciding as closely as possible with the times of the radiation observations were constructed on the basis of National Weather Center analyses. The composite nephanalyses separate overcast (including fog and obscured-sky), broken, and clear-to-scattered areas. The lack of data over many oceanic and tropical areas limits both types of composite analysis.

First the radiation maps were drawn as completely and independently as possible, and then the composite nephanalyses were drawn. In areas north of 35°–40° N, where data were sufficient for independent radiation analyses and nephanalyses, the close relationship between the two was apparent. Hence, the nephanalyses, if available, were used to supplement the radiation analyses for local areas where radiation data were sparse. Despite the limitations of this method, it was used in these early radiation maps in order to permit as much study as possible of their potential value. With increased observational density completely independent radiation maps can be drawn.

It is interesting also to note that in those large portions of the oceans and tropics where no surface observations are available for nephanalyses, the major source of data was the satellite's radiation observations. However, because of the large gaps between orbital paths in the tropics, interpolation in drawing isolangleys is difficult. Here, 24-hour continuity in radiation observations would prove invaluable.

Characteristics of Radiation Maps

That clouds dominate the formation of the radiation pattern is apparent when radiation analyses (Fig. 2) are compared with associated nephanalyses (Fig. 3) for areas north of 40° N. Since the extensive mid-latitude cloud systems of variable vertical development are caused by surface low-pressure centers and fronts, the resulting radiation-map patterns also reflect these sources. Where a surface low or front is most intense, the cloud tops are higher and colder and the amount of outgoing long-wave radiation is smaller. As the cloud tops become lower, the radiating temperature rises and the amount of radiation measured by the satellite sensor increases. On the radiation map, this is seen as a radiation low over the area of maximum cloud development, with higher isolangley values over the area of lower cloud tops. The highest radiation readings are found over the central and eastern sections of surface highs, where clear to scattered-cloud conditions prevail.

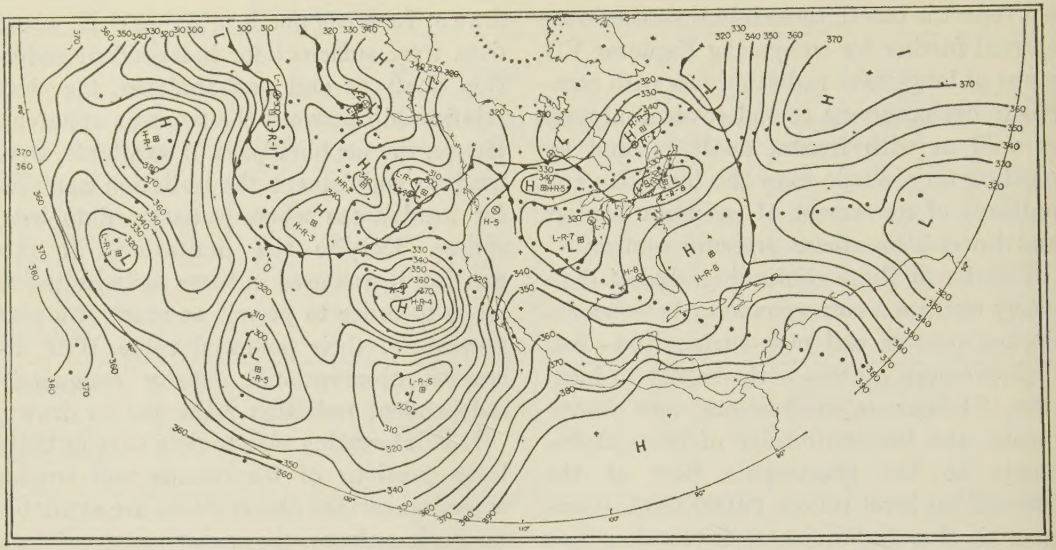

Fig. 2. *Radiation Analysis for Part of Northern Hemisphere, December 1, 1959. Isolangleys show long-wave radiation loss in ly/min* $\times$ 10^{-3}. *Surface-pressure centers (circles marked H or L, for high or low, and numbered) and surface fronts are composite to satellite passage time; radiation centers (squares) are similarly marked but include "R" in designation; dots show observation points and orbital path of satellite.*

From the above relationships, one would expect to find that, in mid-latitudes, the center of the radiation low is east of the surface-low center and the center of the radiation high is east of the surface-high center; this relationship does, in fact, occur in 24 of the 25 cases for which data are available (see Figs. 4 and 5).

In an example of this relationship seen on the maps for December 3, 1959, a radiation low over the Pacific Ocean is located southeast of a surface low and the associated occlusion. Moreover, the orientation of the radiation low and trough (elongated area of low radiation, which may include one or more low centers) parallels the occlusion and the area of maximum frontal intensity, and the radiation pattern's spiral-like northwestward extension resembles Tiros cloud photographs of occlusions.

In addition to indicating frontal location, the radiation trough also indicates frontal intensity and 24-hour frontal changes—the former by the sharpness and strength of isolangley gradient and the latter by the 24-hour change in these factors. An example is the cold front beginning in northwestern Canada from the remnants of an old occlusion and extending southwestward into the Pacific, on December 1, 1959 (Fig. 2). The radiation map correctly indicates that the front is stronger in the region where its clouds produce radiation low L-R-4 and the sharp radiation trough to its southwest; weaker through the area where radiation high H-R-3 is associated with clear to scattered-cloud conditions (Fig. 3); and again more intense as it changes to a warm front leading into the unstable wave of surface pressure low L-1, where the radiation trough strengthens toward L-R-1. A weakening of this radiation trough off the Pacific coast on December 2 reflects decreased activity of the surface cold front.

The entire radiation trough pattern from L-R-4 to L-R-1 and then southwestward resembles a cyclone "family," and, in fact, is the radiation-map reflection of one. The development of family "member" L-1 from an unstable wave to an occlusion can be followed on succeeding radiation maps.

Arrows representing the pattern and location of maximum winds on the US Weather Bureau 0000 GMT 300-mb maps

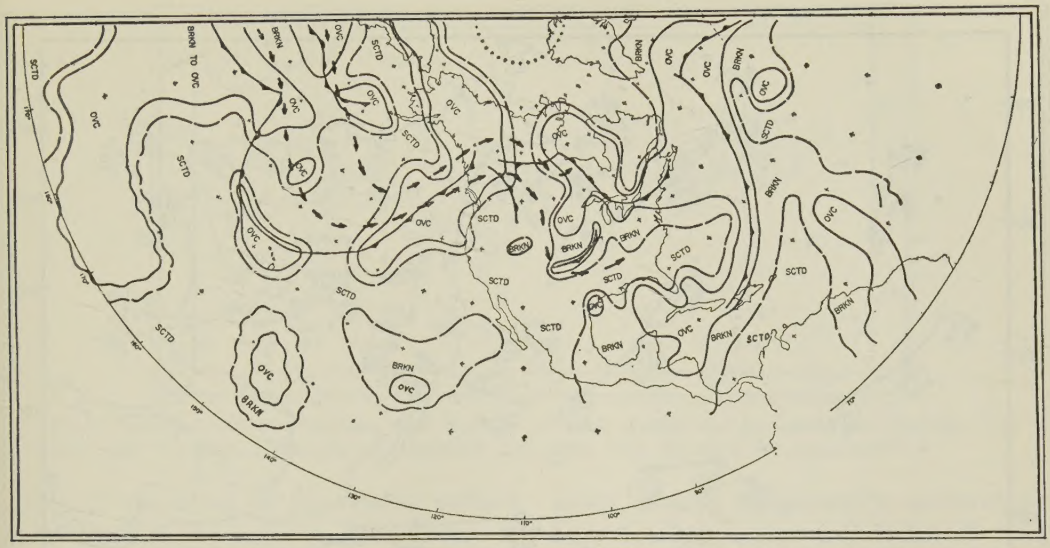

Fig. 3. *Composite Nephanalysis for Part of Northern Hemisphere, December 1, 1959, based on 0000, 0600, and 1200 GMT Surface Maps. Overcast areas (OVC) bounded by solid lines; dash lines separate clear to scattered-cloud (SCTD) areas from broken-cloud areas (BRKN: 5/8–7/8 cloud cover); wavy lines used where cloud-area edge unknown owing to insufficient data; arrows show location and direction of maximum winds, from 300-mb chart for 0000 GMT.*

(about 30,000 feet) are plotted on the nephanalyses. On December 1, 1959, (Fig. 3), the maximum upper-wind and frontal patterns conformed to the pattern shown by other investigators for the relationship of the jet stream to a cyclone family. The patterns of radiation lows and troughs are seen to show the same relationship to the jet stream as do the surface lows and the fronts of the cyclone family.

While radiation lows usually reflect surface lows or fronts, they can also be caused by cold or snow-covered surfaces or by extended sheets of high clouds. Both of these sources may generally be distinguishable by radiation-map analysis and by continuity over several successive radiation maps. No snow surfaces are indicated in the series of maps used in this study, but it seems very likely that extended sheets of high clouds caused those tropical radiation lows that are not related to identifiable synoptic features. (Such large areas of high clouds in the tropics have been reported by a number of other investigators.) It is felt, also, that if sufficient radiation observations are made above an easterly wave, a radiation minimum would be seen over the high clouds in the convergence area. Available synoptic data do not indicate any easterly waves for these dates, however.

24-Hour Intensity Changes

Increases in size, vertical development, and meridional expansion of cloud patterns during the intensification of surface or upper-air lows are reflected in the radiation patterns. In the present study, changes in value of radiation centers reflect the diurnal intensity changes of their surface counterparts for five of eight high centers and for four of six low centers (see Figs. 4 and 5). Reasons for failure to detect this coincidence for the remaining three highs and two lows are difficult to determine, but it is possible that the pressure changes may have been too small to result in changes in clouds and in radiation intensity, or that the clouds may already have been at maximum height. From the limited examples available, it can be stated that in all of the four cases for which the 24-hour change in magnitude of the surface low was greater

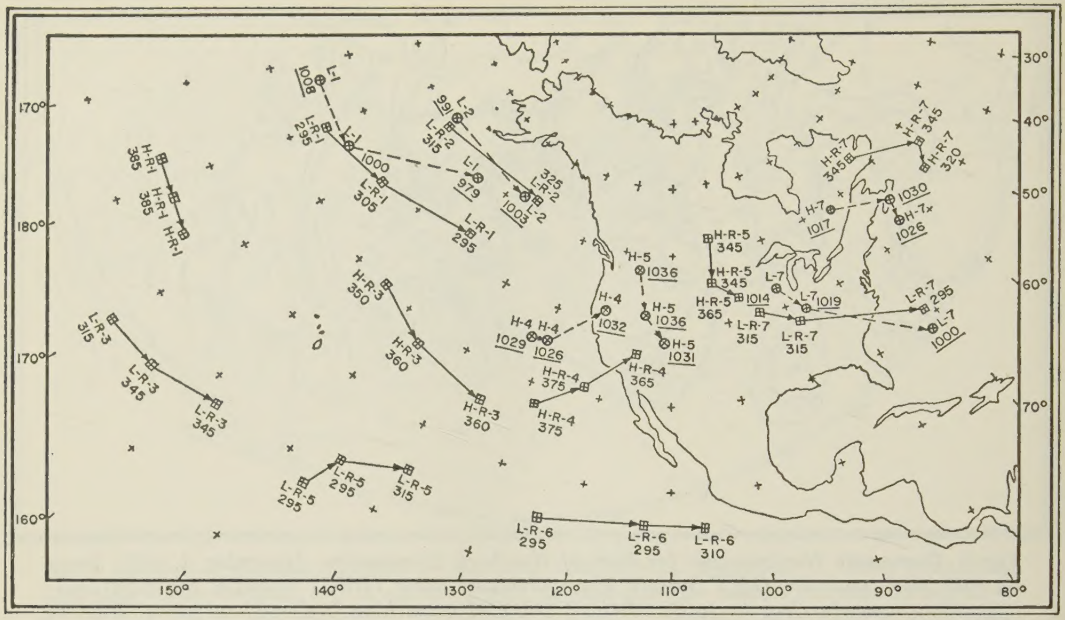

Fig. 4. *Surface- and Radiation-Center Continuity, December 1–3, 1959. Relationships between positions and motions (solid arrows) of radiation centers and positions and motions (dashed arrows) of surface-pressure centers are shown at 24-hour intervals. Radiation values in ly/min* $\times 10^{-3}$*; surface pressures (underlined) in mb.*

than 10 mb, there was a corresponding change in radiation-low intensity.

Intensification of surface centers is also shown by 24-hour shifts in the relative positions of corresponding radiation centers. Radiation low L-R-7, for example, moved from southeast to north-northeast of its corresponding intensifying surface low from December 2 to 3, 1959 (Fig. 4). In another example, limited data for the Pacific indicate that L-R-1 was located east-southeast of surface low L-1 on December 1, moved to the east-northeast of L-1 on December 2, and then to the southeast of this surface low after occlusion took place. On both dates, L-1 deepened (decreased in pressure).

With an intensifying system such as L-1 moving northeastward, some northward motion of the radiation low relative to the surface low (reflecting the movement of highest clouds) would normally be expected. However, on this occasion, the radiation low and trough were apparently in the region of most intense convergence and vertical motion, just ahead of the surface position of the occlusion. It was also noted for the few available examples of surface lows that were either weakening or not changing, that the associated radiation lows retained approximately the same positions relative to the surface lows. L-2 and L-4 and their companion radiation lows are good examples (see Figs. 4 and 5).

Another indication of surface-low intensification based on radiation-map data alone was an observed change in orientation of radiation-low patterns from east-west to north-south coupled with decreases in magnitude of the radiation center. The reverse applied to weakening systems.

24-Hour Motion and 500-mb Geostrophic Flow

Figures 4 and 5 show a possibly useful relationship between the 24-hour movements of mid-latitude surface lows and highs and the movement of associated radiation lows and highs. The 24-hour motions of six out of seven radiation highs remained within about 20° of the direction of motion and 10

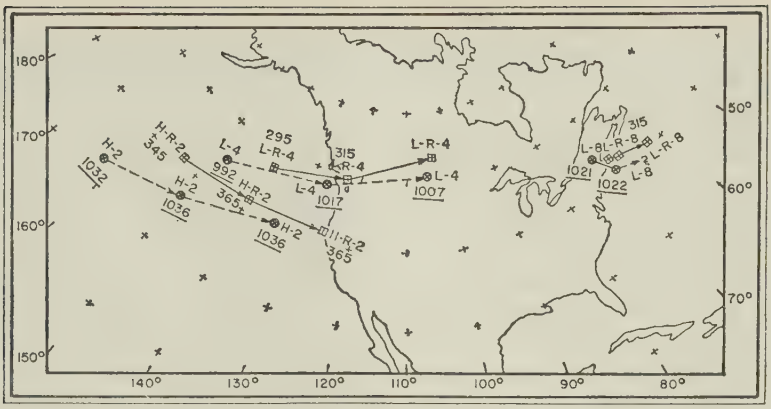

Fig. 5. *Comparison of Positions and Motions of some Additional Radiation and Surface Centers over Northern Hemisphere, December 1–3, 1959. (See Figure 4 for explanation.)*

knots of the speed of the related surface systems. For the seventh, comparison is complicated by absorption of the surface high by another high. Nevertheless, the 24-hour movements of all seven radiation lows followed the movements of their associated surface lows within these limits.

A positive relationship was found between the 24-hour motion of radiation-low centers and the average 500-mb geostrophic wind velocity over their areas of motion. Using computations made from contour spacings on the National Weather Analysis Center 500-mb maps for December 1–4, 1959, it was found that the motions of four of seven radiation highs were within 20° of the direction and 40–60% of the speed of the related 500-mb geostrophic wind. The motions of radiation lows show even better correlation, with six of the seven remaining within these limits.

The above results indicate that the motion of the center of a radiation low could be used to determine the 500-mb flow pattern and the approximate location of the corresponding surface-low center, its movement, and possible changes in its intensity.

Cirrus clouds causing the tropical radiation lows were probably at altitudes between 12 and 16 kilometers. Although the 500- and 300-mb analyses extend only to latitudes of 15°–20° N, the contour pattern indicates that the flow of the westerlies continued farther south at these and higher levels, causing the generally eastward motion of radiation centers H-R-1, L-R-5, and L-R-6 (Fig. 4). L-R-3 could have been under the influence of the equatorial westerlies which, according to previous studies can extend to a height of 16 km. These subtropical centers also showed good continuity—i.e., smoothness of change of character with time and distance.

Summary and Conclusions

The long-wave radiation measurements made by the relatively simple, omnidirectional, white sensor installed aboard Explorer VII can be used to produce radiation maps contoured in ly/min. Analysis techniques are similar to those now used for surface and upper-air maps. In mid-latitudes, where adequate data exist for analysis, the radiation pattern was found to be consistent with the nephanalysis pattern and with synoptic features.

The radiation map appears to offer many aids to weather analysis and forecasting, particularly for areas of sparse data. The best results are obtained for mid-latitudes, for which radiation-low centers approximate the locations, motions, and intensity changes of corresponding surface-low centers. In addition, in limited areas where the direction of motion of a radiation low can be determined, the upper-air pattern and 500-mb winds may be approximated. A special

synoptic situation, the cyclone family, is also recognizable in analysis of radiation patterns, and the general location of the associated maximum winds may be determined. In all latitudes, the radiation analysis, whether determined by radiation data alone, nephanalysis alone, or a combination of both, shows good continuity.

It may be possible in these investigations to determine patterns of vertical motion from the radiation-map patterns, particularly if the low-resolution, quantitative radiation-map values from Explorer VII are combined with high-resolution, qualitative cloud pictures from a Tiros satellite. (Research on this technique is now being conducted at the University of Wisconsin.)

If two satellites were used to make radiation measurements, observation density would be increased and the resulting mats would be more nearly synoptic; polar-orbit satellites having data-storage capability could give global coverage—depending on number and locations of read-out stations.

Energetic-Particles Satellite: Explorer XII

Explorer XII, instrumented to measure energetic particles and magnetic fields to distances greater than 10 earth radii, was launched from Cape Canaveral, Florida, at 11:21 pm EDT, August 15, 1961. (See Figure 6.) The satellite entered a highly eccentric orbit, as planned, with apogee at a distance from the earth of approximately 77,340 kilometers (47,950 statute miles); perigee at about 294 km (182 statute miles); orbital inclination of 33° with respect to the equator; and orbital period of 26 hours 25 minutes.

Explorer XII is the first of several energetic-particles satellites designed specifically to make repeated observations of the solar wind; interplanetary magnetic fields; distant regions of the earth's magnetic field; and the charged-particle population of interplanetary space and of auroral radiation and the trapped-radiation regions near the earth (the Van Allen Radiation Belts). The Van Allen belts, which surround the earth between north and south latitudes of 70° and between distances of about 1000 and 50,000 km are traversed twice during each orbit of the satellite. (See Figure 7.)

With its highly eccentric orbit, Explorer XII provides a unique opportunity to study the physics of fields and energetic particles in space. At apogee, the satellite is essentially in interplanetary space beyond the earth's effective magnetic field; as it moves away from apogee, the satellite passes through the trapped radiation regions; and at perigee it is located below these regions.

The experiments aboard Explorer XII have been carefully selected to cover the particle spectra from energies of a few ev to 10^9 ev. Simultaneous magnetic-field measurements extending to a lower limit of several gammas will also be made, and a solar plasma probe has been provided.

NASA's Goddard Space Flight Center has the major responsibility for the Explorer XII energetic-particles satellite, for its integration with the Delta launch vehicle, and for tracking and data reduction. NASA Project Manager for Explorer XII is Paul Butler, of Goddard, and Frank B. McDonald, also of Goddard, is Scientific Advisor. John E. Naugle is chief of NASA's Energetic Particles Program.

The Explorer XII cosmic-ray, ion-electron-detector, and solar-cell experiments

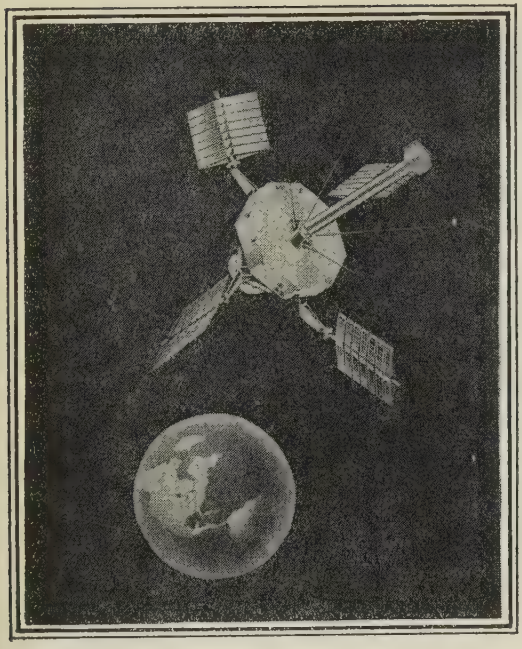

Fig. 6. *Explorer XII Energetic-Particles Satellite (1961 Upsilon). NASA drawing.*

are being conducted by the Goddard Space Flight Center under the direction, respectively, of F. B. McDonald, L. R. Davis, and G. W. Longanecker. The proton-analyzer experiment, is conducted by NASA's Ames Research Center, under the direction of Michael Bader. Lawrence Cahill directs the magnetometer experiment of the University of New Hampshire, and B. J. O'Brien directs the State University of Iowa experiment to measure trapped and solar particles and cosmic rays.

Approximately 50 private contractors also participated in the Explorer XII project and are contributing to NASA's Energetic Particles Program.

As soon as it was affirmed that Explorer XII had entered a stable orbit, a message containing basic information about payload characteristics, experimental aims and instrumentation, and orbital details was sent to COSPAR for distribution to participating national organizations. Scientific information obtained by the satellite is also being sent to COSPAR for similar distribution and is being deposited in the World Data Centers.

NASA's Energetic Particles and Fields Program

NASA's Energetic Particles and Fields Program is concerned with rocket, satellite, and space-probe studies of charged particles having energies greater than a few electron volts. These include solar and galactic cosmic rays, magnetically trapped radiation in the vicinity of the earth and planets, and interplanetary plasmas. The interaction between charged particles and magnetic fields in space is such that both must be studied simultaneously on the same spacecraft. In addition to mapping fields and particle fluxes in space, it is hoped that the data obtained in these studies will provide answers of fundamental questions concerning the origin and method of acceleration of cosmic rays, the nature of the interplanetary magnetic field, and the mechanism responsible for planetary magnetic fields.

It is also necessary, in order to understand certain of these phenomena, to obtain simultaneous measurements at widely separated points in the solar system. Particle and field experiments are therefore planned for deep-space probes such as Ranger and Mariner.

Certain of these phenomena are related to the 11-year solar cycle and must be monitored carefully through an entire cycle. At present, we are in a transition period between the high solar activity of 1957–58 (the IGY period) and the solar minimum expected to occur in 1964–65 (the planned IQSY period; see *Bulletin No. 48*).

Specific areas of investigation of NASA's energetic-particles program are as follows:

Cosmic Radiation: Primary cosmic radiation consists of a continuous flux of protons (H^+), alpha particles (He^{++}), and the nuclei of heavier atoms, and ranges in energy from a few million electron volts to about 10^{19} ev, or more. The flux varies by a factor of almost two over the 11-year

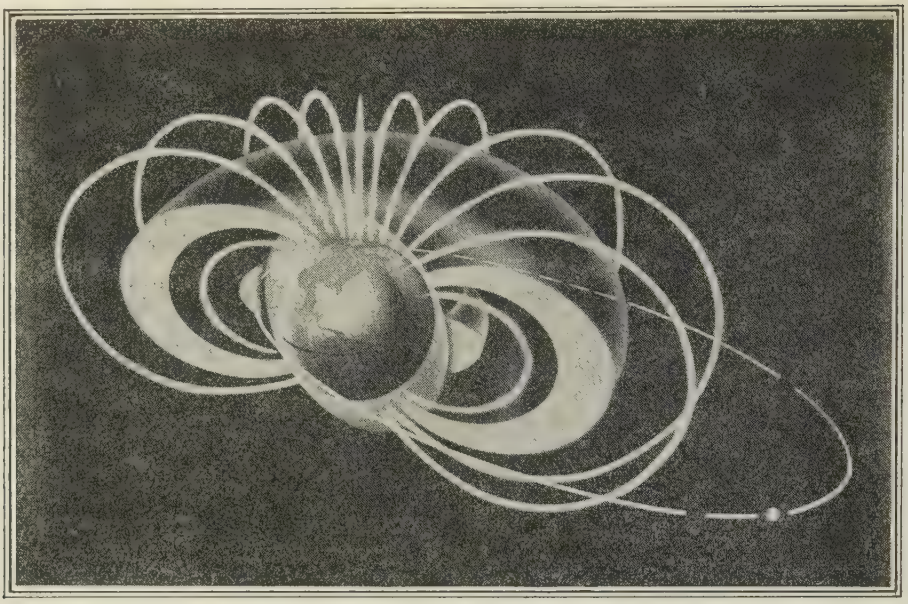

Fig. 7. *Schematic Representation of Explorer XII Orbit. Position of orbit relative to Van Allen Radiation Belts, geomagnetic field, and earth's atmosphere are shown. NASA drawing.*

solar cycle, occasionally decreasing sharply for a few days after a solar flare—the so-called Forbush decrease. The origin of cosmic-ray particles, the mechanism by which they are accelerated to very high energies, their association with the 11-year solar cycle, and the Forbush modulation of the flux and energy spectrum are some of the problems that have shaped this part of the experimental program.

Very-high-energy primary cosmic rays are galactic, or in some cases extragalactic, in origin and pour toward the earth continuously and from all directions. The lower-energy solar cosmic radiation is detected as proton bombardments of the earth's polar regions following solar flares and lasting from a few hours to several days. For a better understanding of solar cosmic rays, following areas required experimental and theoretical investigation: (i) composition, flux, and energy spectra of the particles, and the variations of these quantities with time and position during a solar-cosmic-ray event; (ii) the nature of the solar mechanism that accelerates these particles to high energies and the relation between this mechanism and other solar phenomena; (iii) the trajectories of the particles and their distribution in space during an event; (iv) variation of the frequency and intensity of solar-cosmic-ray events over an entire 11-year solar cycle; and (v) radiation levels in space.

Auroral and Geomagnetically-Trapped Radiation: The geomagnetically trapped and auroral radiation are both associated with the earth's great radiation belts. The Van Allen Radiation Belts consist of two major regions—an inner region, stable with time and characterized by a high density of protons with energies ranging from a few Mev to about 700 Mev, and an outer region, varying with time and consisting of particles with energies of less than one Mev. It is believed that a mechanism in the vicinity of the earth accelerates the particles trapped in the belts. In addition, measurements made during the IGY have shown that both low-energy protons and electrons are associated with auroras, the major part of the incident energy being carried by the electrons.

Some of the primary questions in this

area concern: (i) origins of the radiation in various regions of the Van Allen belts; (ii) lifetimes and trajectories of the trapped and auroral particles; (iii) nature of the local accelerating mechanism; (iv) relation between the trapped and auroral radiation; (v) effects of this radiation on the earth's atmosphere and ionosphere; and (vi) the possible existence and nature of similar belts around the other planets and the moon.

Interplanetary Plasma: The energetic-particles program is investigating fundamental questions about the interplanetary plasma relating to (i) composition of the particles; (ii) their number-density, direction flux, and energy spectra; (iii) relation of these properties to the magnetic field at any point in time and space; and (iv) time variations, ranging from short periods (hydromagnetic waves) to periods of 11 years (solar cycle).

Magnetic Fields: The magnetic-field portion of this NASA program seeks to measure the magnetic fields of the sun, the planets and natural satellites of the solar system, and interplanetary space. Experiments are carried out in conjunction with scientific investigations of the physical processes causing the fields and their changes with time.

Major specific objectives are (i) to survey the entire geomagnetic field in as great detail as possible; (ii) to investigate the sources (presumably ionospheric) of electric current systems giving rise to such ground-observed phenomena as the diurnal magnetic variations (solar and luni-solar), of the more-pronounced variations caused by the equatorial electrojet (see *Bulletin No. 25*), and of magnetic-storm changes, particularly the polar disturbances; (iii) to study the character of the distant portions of the geomagnetic field, including rapid fluctuations possibly related to hydromagnetic waves in the exospheric plasma (Evidence from previous satellites and probes suggested the existence of a ring current [see *Bulletin No. 36*], but uncertainties regarding interpretation of data has made necessary further investigations, in which satellites in eccentric orbits can contribute especially useful information.); (iv) to study the interplanetary magnetic field and its fluctuations, which, presumably, result from the "frozen" fields of plasma clouds ejected from the sun and from hydromagnetic waves traveling through the interplanetary medium; and (v) to study possible magnetic fields of our moon, of Mars and Venus, and, later, of other planets by planned near-misses with space probes, providing information about the existence of such fields and about their character, their approximate magnitude, and the orientation of their poles.

Previous Investigations: Several important experiments have already been completed in the energetic-particles and fields program. Explorer VI, launched August 27, 1959, detected a ring of electrical current circling the earth and mapped the Van Allen Radiation Belts; Vanguard III, launched September 18, 1959, made a large number of accurate magnetic-field measurements in space near the earth (see *Bulletin No. 46*); Explorer VII, launched October 13, 1959, collected data on energetic particles in the Van Allen belts; Pioneer V, launched March 11, 1960, supplied additional data on energetic particles and their distribution as well as on the interplanetary magnetic field (see *Bulletin No. 36*); and Explorer X measured plasmas and magnetic fields in space near the earth (see *Bulletin No. 48*).

Explorer XII Payload Characteristics

The 83-pound Explorer XII satellite carries 10 particle-detecting systems and associated electronics in a 1.578-cubic-foot, octagonal, walled compartment of nylon-honeycomb and fiberglass, with an aluminum cover .02-inch thick. The compartment is 5½ inches high and its side-to-side diameter is 26 5/32 inches. A magnetometer package is located forward of the platform on a 32-inch boom, in order to reduce mag-

netic effects from the electronics and instruments. The transmitter is in the base of the payload.

Four 13.68 × 20.18-inch paddles containing a total of 5600 solar cells extend from the main structure, giving the satellite an over-all diameter of about five feet when in orbit. The paddles, oriented to allow a uniform solar-cell-projection area at any payload-solar attitude, were initially folded along the last-stage rocket and erected during flight. After last stage burnout, a despin device reduced the satellite's roll-rate to approximately 31 rpm and erection of the paddles further reduced it to approximately 18 rpm. Thirteen silver-cadmium storage batteries, recharged by the solar cells, provide 16 watts of power.

Experiments Aboard Explorer XII

The experimental instrumentation aboard Explorer XII is designed to measure particle energies over a range wide enough to include the expected nominal values of the solar wind, the Van Allen Radiation Belts, solar protons, and galactic cosmic rays. Figure 8 shows graphically the energy ranges covered by Explorer XII's detectors, the energy ranges of the various types of particles measured, and the intensity areas in which direct determinations can be made by each detector.

Proton Analyzer: This experiment is designed to measure the low-energy proton flux and spectrum at distances of one quarter to 10 earth radii (about 1500-65,000 km). These particles are believed to make up 85% of the energized particles in space. Data obtained will add to our knowledge of proton concentrations in the solar winds caused by solar flares, and will be useful for correlating particle activity in space and in the Van Allen Radiation Belts with solar activity.

Many scientists consider the interplanetary plasma as simply a continuation of the sun's atmosphere, or corona, consisting mostly of protons and electrons. Others believe that a solar wind—ionized atoms of gas, primarily hydrogen, moving at velocities of several hundred to a thousand miles a second—constantly streams away from the sun. Recent measurements of Explorer X tend to confirm the existence of the solar wind.

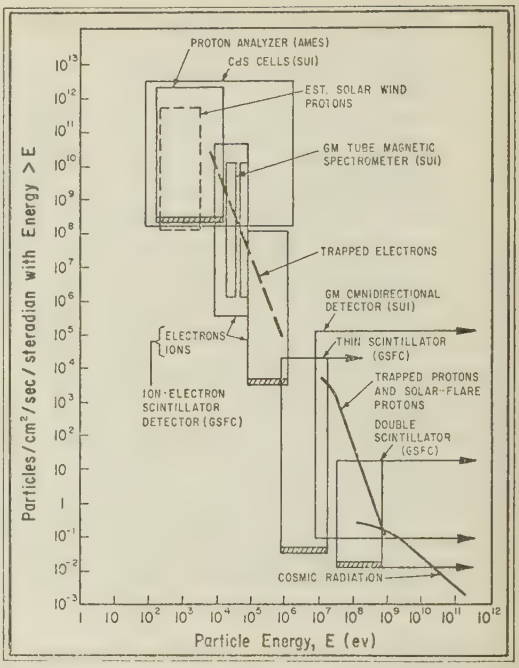

Fig. 8. *Energy-Spectra Ranges of Explorer XII Detectors and of Particles being Measured. Curves represent expected nominal values, as a function of particle kinetic energy, of the solar wind (dashed rectangle, top left); Van Allen region electrons (dashed line); Van Allen region protons and solar protons (upper solid line); and cosmic rays (lower solid line). Solid rectangular areas represent energy and intensity intervals covered by Explorer XII instrumentation. All detectors have large dynamic ranges to allow for expected fluctuations; cross-hatched areas indicate intensity intervals in which particle-energy spectra can be determined directly.*

The plasma probe in Explorer XII, designed and built at Ames, records the presence of particles as a function of their energy, in the range 200 ev–20 kev, which corresponds to the expected 200- to 2000-km/sec velocity range. Charged particles enter the analyzer through a slit in the sat-

ellite skin opening into a curving tunnel. The two sides of the tunnel are metal plates carrying static electric charges, one negative and the other positive. A charged particle is attracted by one plate and repelled by the other, and so follows the curved path down the tunnel. If it is moving either too slowly or too rapidly it runs into one wall or the other, but if it is within the right velocity range, it makes its way to the particle counter at the end of the tunnel. Thus, all particles moving in a particular direction and within the desired velocity range are detected. At fixed intervals the range of energies is changed.

Magnetic Fields: This experiment measures the magnitude and direction of the earth's magnetic field at distances between 3 and 10 earth radii (approximately 20,000-65,000 km). It is also investigating the possible termination of the geomagnetic field in the vicinity of 10 earth radii. The data gathered will determine whether postulated current systems and magnetic disturbances actually exist in extraterrestrial space, particularly in association with solar events and changes in particle intensities.

Several satellite and space-probe measurements have already provided some information about the geomagnetic field and the interplanetary magnetic field between the earth and the moon, where these fields interact to form a complicated boundary.

The flux-gate magnetometer used for these Explorer XII measurements is a three-core device. Each of three orthogonal sensors measures a magnetic field element along that sensor. The output voltages of the sensors are then combined to form the total-magnetic-field vector. The range of measurement is from a few gammas to 1000 gammas.

Trapped-Particle Radiation: The fluxes, energies, and spatial and temporal dependence characteristics of particle radiation—geomagnetically trapped, solar, and cosmic ray—are measured over the entire spacecraft orbit in this experiment.

Instrumentation consists of four Geiger counters and three cadmium-sulphide cells. One counter detects protons with energies above 20 Mev and electrons above 2 Mev, arriving from all directions. The three other Geiger tubes make up an electron spectrometer, one detecting electrons with energies between about 40 and 55 kev, another monitoring penetrating radiations (protons above 50 Mev and electrons above 10 Mev), and the last one measuring electrons between 90 and 100 kev.

The cadmium-sulphide cells are solid-state, semi-conductor devices that change their electrical resistance in proportion to the rate of bombardment by charged particles. One cadmium-sulphide cell measures the total energy flux of both protons and electrons down to energies of 100 ev, or less. Another has a magnet that deflects electrons below several hundred kev, thus measuring only the low-energy protons. The third cadmium-sulphide cell is fitted with a transparent shield so that accurate corrections may be made for the effects of light (earthlight or sunlight) striking the other two cells.

Cosmic Rays: The Explorer XII cosmic-ray monitoring equipment permits study of both the production and modulation of cosmic rays with the same set of experiments. Charge and energy spectra of the cosmic radiation are measured as a function of distance from the earth, time, and direction.

The cosmic-ray package consists of three basic detection units: a double scintillation-counter telescope, a single crystal detector, and a Geiger-Mueller telescope. The first detector measures the total cosmic-ray flux; the flux of fast protons with energies greater than 700 Mev; the differential energy spectrum of protons in the region 70–750 Mev; and the low-energy portion of the alpha-particle differential-energy spectrum.

In order to extend the proton energy-spectrum data down to 1 Mev, a thin cesium-iodide scintillation counter is used as the second detection unit. The pulse-height distribution of incident particles in the energy range 100 kev–20 Mev is ob-

tained. This unit also provides information on low-energy solar gamma rays.

The third unit, the Geiger-Mueller telescope, consists of two Geiger counters that serve as cosmic-ray monitors, furnishing a check on the information received from the scintillation-counter units.

Ion-Electron Detector: This detector measures particle fluxes, types, and energies —as a function of direction, time, and position—below, in, and above the Van Allen Radiation Belts. The detector is most sensitive to the low-energy particles, which, although they have not yet been measured directly, appear to exist in both the inner and outer radiation belts.

The ion-electron scintillation detector consists of a powder phosphor on a photomultiplier tube located behind a stepping absorber wheel. Ion counting rates for two trigger levels are registered with respect to seven absorber thicknesses, from which ion types and energy spectra can be deduced. The electron energy flux is also obtained, and electron energy spectra can be deduced by comparing the responses from six absorber thicknesses. Total energy flux is obtained for seven absorber thicknesses by measuring the photo-multiplier current.

The ion detector measures protons in the energy range 0.1 kev-1 Mev; the electron detector records within the energy range 10-100 kev; and the total-energy-flux detector functions over the energy range of 30 kev to 1 Mev for protons and 10-100 kev for electrons.

Solar Cells: Deterioration of solar cells from direct exposure to the Van Allen radiation is investigated in this experiment. Four strips of silicon solar cells, with 10 cells per strip, are mounted on the surface of the spacecraft. One strip is unprotected while the remaining three are protected by 3-, 20-, and 60-mil-thick glass filters. During the lifetime of the spacecraft, the effectiveness of the different thicknesses of glass in preventing deterioration of the cells will be compared.

Optical-Aspect Sensor: Explorer XII carries an optical-aspect sensor to determine its orientation in space as a function of time. Six photo-diodes give the sun's elevation with respect to the spin axis of the satellite. The photo-diodes are placed behind a light mask so that each sees only the portion of the light mask directly in front of it, and a digital computer having memory and logic capabilities, determines the time at which a particular photo-diode sees the sun.

Telemetry

A 2-watt, 136.02-megacycle transmitter operates continuously in Explorer XII. Because of its highly eccentric orbit, the satellite is visible for approximately 23 hours at receiving stations on the apogee side of the earth. Three stations, at Woomera, Australia, Santiago, Chile, and Johannesburg, South Africa, are spaced in longitude such that, together, they can record the telemetry signal for 90% of the time. Initial plans were to record telemetry continuously for one month and periodically thereafter as required.

Tracking

Tracking Explorer XII on the apogee side of the orbit are the existing Minitrack stations at Woomera; Johannesburg; Santiago; Antofagasta, Chile; and Lima, Peru. The rapid passes of the satellite through perigee are tracked as the satellite crosses existing Minitrack stations such as Blossom Point, Maryland; Fort Myers, Florida; and Goldstone, California.

Initial Results

Acquisition of telemetry data from Explorer XII has been satisfactory, and during the 100%-coverage period (through November 1961), approximately 3000 magnetic tapes (each 2400 feet long) per month were recorded by the Minitrack network. It was planned to reduce coverage to 25%

in December, subject to technical requirements. Only one-third of the data tapes can be processed as received, but a statistical sample of the telemetry records is analyzed at that time. Data obtained near the time of more-prominent solar flares and magnetic storms have been given priority.

The principal investigators for the various experiments have reduced sufficient data to report that observed intensities appear to be within the expected ranges. Data from the ion-electron-detector experiment indicates a definite termination of the outer edge of the outer Van Allen region.

Between August 15 and September 12, 1961, the spin rate of the satellite increased from 27.78 rpm to 28.63 rpm (approximately 2.7%). This increase has been attributed to the effect of solar-radiation pressure on the four solar paddles, which are pitched in the proper direction to aid the spin rate when the sun is shining on the lower half of the satellite. This effect was expected to continue for the first 160 days following launch.

A major degradation in the output of the unprotected solar-cell test patch has been observed, totalling 50% from August 16 to 18, 1961, and an additional 35% from August 18 to September 14. No degradation was noticeable for the three covered test-cell patches.

The orbital parameters for Explorer XII have changed as a result of solar and lunar perturbations. By September 12, apogee had decreased to approximately 77,030 km (47,863 statute miles) and perigee had increased to about 447 km (278 statute miles). The increase of perigee and decrease of apogee is as predicted and does not compromise the one-year lifetime needed for the Explorer XII experiments.

Bibliographic Notes

Akasofu, S.-I., Chapman, S., The ring current, geomagnetic disturbance, and the Van Allen radiation belts. *Journal of Geophysical Research, 66*(5), 1321–1350, May 1961.

Arnoldy, R. L., Hoffman, R. A., Winckler, J. R., Measurements of the Van Allen radiation belts during magnetic storms. *Space Research,* H. K. Kallmann-Bijl, ed., North-Holland Publishing Co., 877–96, 1960 (*IGY Satellite Report No. 11,* 89–104. 1960).

Benes, N. S., Inside Antarctica No. 4—The Hallett Story. *Weatherwise, 12*(5), 200–205, October 1959.

Cartwright, G. D., Rubin, M. J., Inside Antarctica No. 6—Meteorology at Mirny. *Weatherwise, 14*(3), 110–118, June 1961.

Coleman, P. J., Jr., The effects of betatron accelerations upon the intensity and energy spectrum of magnetically trapped particles. *Journal of Geophysical Research, 66*(5), 1351–61, May 1961.

Fan, C. Y., Meyer, P., Simpson, J. A., Trapped and cosmic radiation measurements from Explorer VI. *Space Research,* H. K. Kallmann-Bijl, ed., North-Holland Publishing Co., 951–66, 1960 (*IGY Satellite Report No. 11,* 115–25, 1960).

Flowers, Edwin, Inside Antarctica No. 2—Amundsen-Scott Station. *Weatherwise, 11*(5), 166-171, 180, October 1958.

Harlin, B. W., Inside Antarctica No. 1—Little America. *Weatherwise, 11*(2), 115–123, August 1958.

Hess, W. N., Killeen, J., Fan, C. Y., Meyer, P., Simpson, J. A., The observed outer-belt electron distribution and the neutron decay hypothesis. *Journal of Geophysical Research, 66*(8), 2313–14, August 1961.

IGY World Data Center A: Rockets and Satellites, Corpuscular radiation, magnetic field, and micrometeorite observations with satellites and space probes. *IGY Satellite Report No. 14,* National Academy of Sciences, 193 p., July 1961.

King, G. A. M., Roach, F. E., Relationship between red auroral arcs and ionospheric recombination. *Journal of Research, 65D*(2), 129–35, March-April 1961.

Liemohn, H., The outer radiation belt and aurorae. *Nature, 188*(4748), 394–95, October 29, 1960.

Moreland, W. B., Inside Antarctica No. 3—The Weather Central at Little America. *Weatherwise, 11*(6), 196–200, December 1958.

Morris, W. R., Peters, N. L., Inside Antarctica No. 5—Byrd Station. *Weatherwise 13*(4), 162–165, August 1960.

Ney, E. P., Experiments on cosmic rays and re-

lated subjects during the International Geophysical Year. *Annual Review of Nuclear Science, 10,* 461–88, 1960.

Parker, E. N., Geomagnetic fluctuations and the form of the outer zone of the Van Allen radiation belt. *Journal of Geophysical Research, 65*(10), 3117–30, October 1960.

Reid, G. C., Rees, M. H., Speculations on the connection between the Van Allen radiation and the aurora. *Proceedings of the Symposium on Physical Processes in the Sun-Earth Environment, July 20–21, 1959,* C. Collins, comp., DRTE Publication 1025, Defence Research Board, Ottawa, 361–71, 1960.

Rosen, A., Farley, T. A., Sonnett, C. P., Soft radiation measurements on Explorer VI earth satellite. *Space Research,* H. K. Kallmann-Bijl, ed., North-Holland Publishing Co., 938–50, 1960 (*IGY Satellite Report No. 11,* 105–14, 1960).

Rothwell, P., Satellite observations of solar cosmic rays and other low altitude charged particle intensity variations. *Proceedings of the Symposium on Physical Processes of the Sun-Earth Environment, July 20–21, 1959,* C. Collins, comp., DRTE Publication 1025, Defence Research Board, Ottawa, 303–10, 1960.

Sonett, C. P., Smith, E. J., Sims, A. R., Surveys of the distant geomagnetic field: Pioneer I and Explorer VI. *Space Research,* H. K. Kallmann-Bijl, ed., North-Holland Publishing Co., 921–37, 1960 (*IGY Satellite Report No. 14,* 107–23, 1961).

Singer, S. F., Latitude and altitude distribution of geomagnetically trapped protons. *Physical Review Letters, 5*(7), 300–3, October 1, 1960.

Preprinted from *Transactions, American Geophysical Union,* Vol. 42, No. 4, Dec., 1961